



# Effect of adaptive statistical iterative reconstruction-V (ASiR-V) levels on ultra-low-dose CT radiomics quantification in pulmonary nodules

Kai Ye<sup>1</sup>, Min Chen<sup>2</sup>, Qiao Zhu<sup>1</sup>, Yuliu Lu<sup>1</sup>, Huishu Yuan<sup>1</sup>

<sup>1</sup>Department of Radiology, Peking University Third Hospital, Beijing, China; <sup>2</sup>Department of Radiology, Ghent University Hospital, Corneel Heymanslaan 10,9000, Ghent, Belgium

*Correspondence to:* Huishu Yuan. Department of Radiology, Peking University Third Hospital, 49 North Garden Road, Haidian District, Beijing 100191, China. Email: huishuy@bjmu.edu.cn.

**Background:** The weightings of iterative reconstruction algorithm can affect CT radiomic quantification. But, the effect of ASiR-V levels on the reproducibility of CT radiomic features between ultra-low-dose computed tomography (ULDCT) and low-dose computed tomography (LDCT) is still unknown. The purpose of study is to investigate whether adaptive statistical iterative reconstruction-V (ASiR-V) levels affect radiomic feature quantification using ULDCT and to assess the reproducibility of radiomic features between ULDCT and LDCT.

**Methods:** Sixty-three patients with pulmonary nodules underwent LDCT (0.70±0.16 mSv) and ULDCT (0.15±0.02 mSv). LDCT was reconstructed with ASiR-V 50%, and ULDCT with ASiR-V 50%, 70%, and 90%. Radiomics analysis was applied, and 107 features were extracted. The concordance correlation coefficient (CCC) was calculated to describe agreement among ULDCTs and between ULDCT and LDCT for each feature. The proportion of features with CCC >0.9 among ULDCTs and between ULDCT and LDCT, and the mean CCC for all features between ULDCT and LDCT were also compared.

**Results:** Sixty-three solid nodules (SNs) and 48 pure ground-glass nodules (pGGNs) were analyzed. There was no difference for the proportion of features in SNs among ULDCTs and between ULDCT and LDCT ( $P>0.05$ ). The proportion of features in pGGNs were highest for ULDCT<sub>70% vs. 90%</sub> (78.5%) and ULDCT<sub>90% vs. LDCT<sub>50%</sub></sub> (50.5%). In SNs, the mean CCC for ULDCT<sub>90% vs. LDCT<sub>50%</sub></sub> was 0.67±0.26, not different with that for ULDCT<sub>50% vs. LDCT<sub>50%</sub></sub> (0.68±0.24) and ULDCT<sub>70% vs. LDCT<sub>50%</sub></sub> (0.64±0.21) ( $P>0.05$ ). In pGGNs, the mean CCC for ULDCT<sub>90% vs. LDCT<sub>50%</sub></sub> was 0.79±0.19, higher than that for ULDCT<sub>50% vs. LDCT<sub>50%</sub></sub> (0.61±0.28) and ULDCT<sub>70% vs. LDCT<sub>50%</sub></sub> (0.76±0.24) ( $P<0.05$ ).

**Conclusions:** ASiR-V levels significantly affected ULDCT radiomic feature quantification in pulmonary nodules, with stronger effects in pGGNs than in SNs. The reproducibility of radiomic features was highest between ULDCT<sub>90%</sub> and LDCT<sub>50%</sub>.

**Keywords:** Computed X-ray tomography; radiomics; pulmonary nodule; ASiR-V; reproducibility

Submitted Jul 31, 2020. Accepted for publication Dec 22, 2020.

doi: 10.21037/qims-20-932

**View this article at:** <http://dx.doi.org/10.21037/qims-20-932>

## Introduction

In recent years, the development of computational power and image feature extraction has led to the use of high-throughput extraction of quantitative imaging features combined with different kinds of diagnostic models to assist clinical decisions, in a process called radiomics (1,2). Extensive research indicates that radiomics has shown promise in pulmonary nodule characterization, histopathologic staging, prognostic analysis, and recognition of gene mutations (3-7).

At present, chest low-dose computed tomography (LDCT) is the recommended modality for screening non-small cell lung cancer (NSCLC) (8). In addition to monitoring the size of pulmonary nodules, LDCT is also widely used in radiomics analysis (9-11). Owing to developments in computed tomography, the wide applicability of iterative reconstruction (IR) algorithms has enabled the realization of ultra-low-dose CT (ULDCT), which has a lower radiation dose than LDCT. The radiation dose of ULDCT is  $<0.2$  mSv, which is comparable with the dose of chest radiography (12-14). As a third-generation IR, adaptive statistical iterative reconstruction-V (ASiR-V) has the ability to reduce image noise and is widely adopted in the image reconstruction of ULDCT (15,16).

Recently, there have been many reports on the reliability of ULDCT for screening NSCLC, with some researchers even recommending replacing LDCT with ULDCT for NSCLC screening (17-20). Nevertheless, these studies focused on conventional image diagnosis by the naked eye and ignored the ULDCT radiomic quantification in pulmonary nodules *in vivo*. The reproducibility of CT radiomic features between LDCT and ULDCT remains unknown. Moreover, some studies have shown that changing the weightings of IR can affect the reproducibility of CT radiomic features (21). However, there are only a few studies on the effect of IR algorithms on CT radiomic quantification considering the high number of commercial IR algorithms that are composed of different models (22-26). The effect of changing the weightings for different IR algorithms on the reproducibility of CT radiomic features needs to be investigated further.

Therefore, this study aimed to evaluate the variability of quantification of radiomic features computed using ULDCT reconstructed with different ASiR-V levels and investigate the effect of ASiR-V levels on the reproducibility of CT radiomic features between ULDCT reconstructed with different ASiR-V levels and LDCT, by assessing the

agreement of CT radiomic features (including first-order statistical, textural, and structural features) among ULDCTs with different ASiR-V levels as well as the agreement between ULDCT and LDCT in pulmonary nodules.

## Methods

### *Participants*

From August 2019 to January 2020, we enrolled patients who underwent LDCT for pulmonary nodule follow-up in our radiology department. The inclusion criteria were as follows: (I) age  $\geq 18$  years and body mass index (BMI)  $\leq 35$  kg/m<sup>2</sup>, (II) acceptable diagnostic image quality of LDCT, (III)  $\leq 5$  pulmonary nodules without calcification, and (IV) solid nodules (SNs) and pure ground-glass nodules (pGGNs) with diameters of 4–15 mm (the diameter was calculated as the mean of the longest diameter and perpendicular diameter of a nodule) (27). The exclusion criteria were as follows: (I) LDCT with the tube voltage of 100 kV, (II) patients with diffuse consolidation and/or other diseases, making pulmonary nodules unevaluable, and (III) patients with pulmonary part-solid nodules (PSNs).

There were 85 patients in the preliminary study. Among them, twenty-two patients were excluded (three patients with poor image quality of LDCT, five patients with PSNs and fourteen patients scanned with tube voltage of 100 kV). Finally, our study population consisted of 63 patients [14 men, 49 women; mean age,  $55.0 \pm 13.2$  (range, 23–82) years; mean BMI,  $22.67 \pm 2.95$  (range, 17.5–31.14) kg/m<sup>2</sup>].

This study was approved by the institutional review board of our department, and informed consent was obtained from the participants.

### *CT acquisition and reconstruction*

All CT scans were performed on a revolution CT scanner (GE Healthcare, Milwaukee, WI, USA) and conducted with the patient in a deep inspiratory breath-hold. Patients were scanned using a conventional non-enhanced LDCT protocol, immediately followed by ULDCT. The interval between the two protocols was  $<1$  min. All scans were used in helical mode, with a scan range from the costophrenic angle to the pulmonary apex.

The LDCT dataset was obtained with a collimation of  $64 \times 0.625$  mm, beam pitch of 0.984:1, Assist tube voltage of 120/100 kV, Smart mA with a noise index of 14.1 HU (min/max mA, 50/680), and gantry rotation time of 0.28 s.

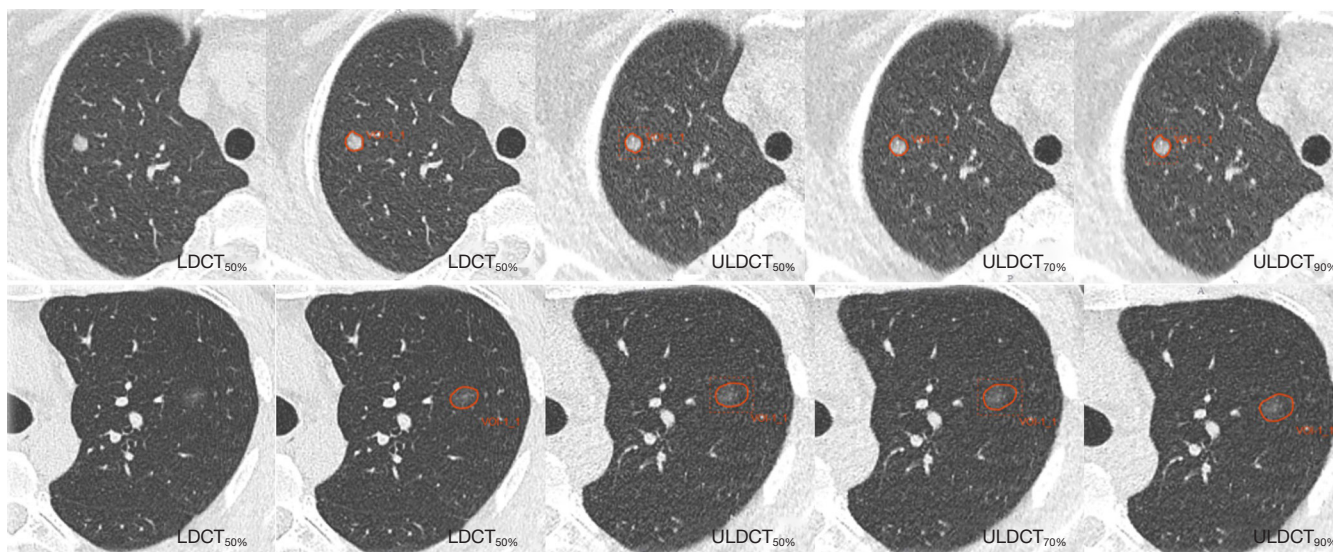


**Figure 1** Process of nodule segmentation for both solid nodule and pure ground-glass nodule. ULDCT<sub>50%</sub>, ultra-low-dose CT (ULDCT) with ASiR-V 50%; ULDCT<sub>70%</sub>, ULDCT with ASiR-V 70%; ULDCT<sub>90%</sub>, ULDCT with ASiR-V 90%; LDCT<sub>50%</sub>, low-dose CT (LDCT) with ASiR-V 50%.

Identical parameters were used for ULDCT, except that the tube voltage was fixed at 120 kV and the tube current was Smart mA with a noise index of 28 HU. LDCT images were reconstructed with ASiR-V 50%, which was described as LDCT<sub>50%</sub>. ULDCT images were reconstructed with ASiR-V 50%, 70%, and 90%, which were described as ULDCT<sub>50%</sub>, ULDCT<sub>70%</sub>, and ULDCT<sub>90%</sub>, respectively. ASiR-V levels used for the image reconstruction of ULDCT were based on the results of our previous study (published in Chinese domestic core journal). All images were obtained using a slice thickness of 1.25 mm with an increment of 1.25 mm. The image matrix was 512×512 pixels.

The mean CT dose index volume (CTDI<sub>vol</sub>) and dose-length product (DLP) for LDCT were 1.4±0.33 mGy and 49.83±11.76 mGy·cm, respectively. The mean CTDI<sub>vol</sub> and DLP for ULDCT were 0.33±0.16 and 11.05±1.7 mGy·cm, respectively. The effective dose (ED) was calculated by multiplying the DLP with a conversion coefficient *k* of 0.014 mSv/mGy/cm (28).

#### ***Nodule segmentation and radiomic feature extraction***

All patient identifiers (including name, age, sex, and medical record number) were removed from the images. Images were presented with a fixed window center of -600 HU and width of 1,600 HU. Image quality of LDCT was

assessed by a radiologist (Doctor A with 5 years' experience in radiology). Images with moderate or mild artefacts which do not affect diagnosis were seen as acceptable. Pulmonary nodule segmentation was performed by two radiologists (Doctor B with 6 years' experience in chest CT and Doctor C with 8 years' experience) in consensus using a semiautomatic segmentation and radiomic feature extraction tool (RadCloud version 3.0; Huiying Medical Technology Co., Ltd.). If the discrepancy of volumes of interest drawn by two doctors was more than 5% (29), the segmentation performed by a third reader (Doctor D with 26 years' experience in chest CT) was chosen. The process of nodule segmentation for both SNs and pGGNs is shown in *Figure 1*.

After nodule segmentation, a total of 107 radiomic features from 3D data were extracted, including histogram, texture and structural features. They included 18 first-order statistical features (histogram), 75 texture features [gray-level co-occurrence matrix (GLCM), gray-level dependence matrix (GLDM), gray-level run length matrix (GLRLM), gray-level size zone matrix (GLSZM), neighboring gray-tone difference matrix (NGTDM)], and 14 structural features (Shape-3D). All of these features were directly extracted from the original images without filtering and can intuitively reflect original information of images. A detailed description of all these 107 features is shown in [Table S1](#).

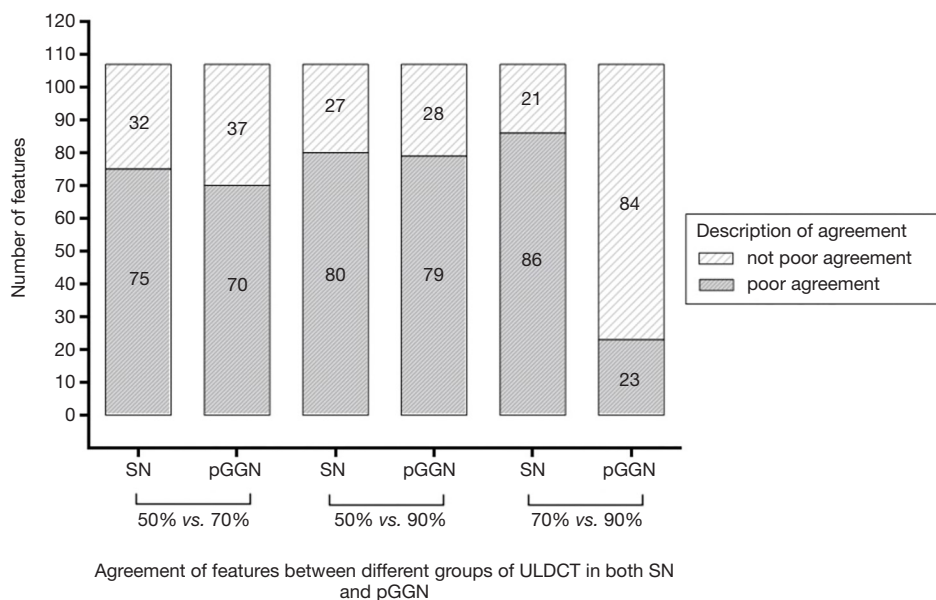


**Figure 2** Agreement of all features between different groups of ultra-low-dose CT (ULDCT) reconstructed with different ASiR-V levels in both solid nodule (SN) and pure ground-glass nodule (pGGN).

### Statistical analysis

Statistical analyses were performed using SPSS version 26.0 (IBM) and MedCalc version 19.0.7.  $P < 0.05$  (two-sided) was considered significant. All radiomic features were regarded as continuous in nature. Continuous variables are reported as mean  $\pm$  standard deviation, and categorical variables as frequencies or percentages. The concordance correlation coefficient (CCC) (30) was calculated to describe the agreement among ULDCTs with different ASiR-V levels and the agreement between ULDCTs with different ASiR-V levels and LDCT for each feature. CCC values of  $>0.99$ ,  $0.95\text{--}0.99$ ,  $0.91\text{--}0.95$ , and  $<0.90$  denoted “almost perfect”, “substantial”, “moderate”, and “poor” agreement, respectively (31). Chi-square statistics were used to compare differences in the proportion of features with CCC  $>0.9$  among ULDCTs with different ASiR-V levels and between ULDCTs with different ASiR-V levels and LDCT. A paired sample t-test was used to compare differences in CCC values for all features between ULDCTs with different ASiR-V levels and LDCT. The 95% confidence intervals of mean CCC values were also calculated.

### Results

A total of 111 nodules were analyzed, including 63 SNs and 48 pGGNs. The mean diameter of SNs was  $5.2 \pm 1.5$  (4.0–

10.4) mm, and that of pGGNs was  $6.1 \pm 1.8$  (4.0–12.0) mm. The ED of ULDCT ( $0.15 \pm 0.024$  mSv) was 78.6% lower than that of LDCT ( $0.7 \pm 0.16$  mSv).

### Agreement between ULDCTs with different ASiR-V levels for all features

The agreement between ULDCTs with different ASiR-V levels for all features in both SNs and pGGNs is shown in Figure 2. In SNs, the proportion of features with CCC  $>0.9$  for ULDCT<sub>50% vs. 70%</sub>, ULDCT<sub>50% vs. 90%</sub>, and ULDCT<sub>70% vs. 90%</sub> was 29.9%, 25.2%, and 19.6%, respectively. There was no obvious difference among them ( $P=0.220$ ).

In pGGNs, features with CCC  $>0.9$  in ULDCT<sub>70% vs. 90%</sub> accounted for 78.5% of all features, significantly higher than that of ULDCT<sub>50% vs. 70%</sub> (34.6%) and ULDCT<sub>50% vs. 90%</sub> (26.2%) ( $P < 0.001$ ). There was no statistical difference in the proportion between ULDCT<sub>50% vs. 70%</sub> and ULDCT<sub>50% vs. 90%</sub> ( $P=0.181$ ).

### Agreement between ULDCTs with different ASiR-V levels and LDCT

The agreement between ULDCTs with different ASiR-V levels and LDCT for all features in both SNs and pGGNs is shown in Table 1. In SNs, the number of features with

**Table 1** Agreement between ULDCCT and LDCT for all features in both SN and pGGN

Variable	Nodule type	ULDCCT <sub>50%</sub> vs. LDCT <sub>50%</sub>		ULDCCT <sub>70%</sub> vs. LDCT <sub>50%</sub>		ULDCCT <sub>90%</sub> vs. LDCT <sub>50%</sub>	
		Poor	Not poor	Poor	Not poor	Poor	Not poor
First-order feature	SN	16	2	15	1	13	3
	pGGN	15	3	8	10	7	11
Shape feature (3D)	SN	6	8	8	6	5	9
	pGGN	7	7	5	9	6	8
GLCM	SN	21	3	22	2	21	3
	pGGN	20	4	16	8	14	10
GLDM	SN	11	3	12	2	10	4
	pGGN	10	4	5	9	6	8
GLRLM	SN	13	3	15	1	14	2
	pGGN	14	2	11	5	9	7
GLSZM	SN	15	1	14	2	15	1
	pGGN	14	2	10	6	7	7
NGTDM	SN	5	0	5	0	5	0
	pGGN	4	1	2	3	2	3

ULDCCT, ultra-low-dose computed tomography; LDCT, low-dose computed tomography; SN, solid nodule; pGGN, pure ground-glass nodule; ULDCCT<sub>50%</sub>, ULDCCT with ASiR-V 50%; ULDCCT<sub>70%</sub>, ULDCCT with ASiR-V 70%; ULDCCT<sub>90%</sub>, ULDCCT with ASiR-V 90%; LDCT<sub>50%</sub>, LDCT with ASiR-V 50%; GLCM, gray-level co-occurrence matrix; GLDM, grey-level difference matrix; GLRLM, gray-level run length matrix; GLSZM, grey-level size-zone matrix; NGTDM, neighborhood grey-tone difference matrix; poor represents poor agreement between this group and LDCT; not poor represents not poor agreement between this group and LDCT.

**Table 2** Comparison of proportions of features with CCC >0.9 between ULDCCT with different ASiR-V levels and LDCT

	ULDCCT <sub>50%</sub> vs. LDCT <sub>50%</sub>	ULDCCT <sub>70%</sub> vs. LDCT <sub>50%</sub>	ULDCCT <sub>90%</sub> vs. LDCT <sub>50%</sub>	$\chi^2$ -value	P value
SN	18.7% (20/107)	13.1% (14/107)	20.6% (22/107)	2.250	0.325
pGGN	21.5% (23/107)*	46.7% (50/107)	50.5% (54/107)	22.227	<0.001

ULDCCT, ultralow-dose computed tomography; LDCT, low-dose computed tomography; CCC, concordance correlation coefficient; ULDCCT<sub>50%</sub>, ULDCCT with ASiR-V 50%; ULDCCT<sub>70%</sub>, ULDCCT with ASiR-V 70%; ULDCCT<sub>90%</sub>, ULDCCT with ASiR-V 90%; LDCT<sub>50%</sub>, LDCT with ASiR-V 50%; SN, solid nodule; pGGN, pure ground-glass nodule. \*The result of this group was different from the other two groups.

different agreements between ULDCCT<sub>50%</sub> and LDCT<sub>50%</sub> was 87 for poor agreement, and 20 for not poor agreement. Between ULDCCT<sub>70%</sub> and LDCT<sub>50%</sub>, there were 93 features with poor agreement, and 14 with not poor agreement. Between ULDCCT<sub>90%</sub> and LDCT<sub>50%</sub>, the number of features was 85 for poor agreement, and 22 for not poor agreement.

In pGGNs, the number of features with different agreements between ULDCCT<sub>50%</sub> and LDCT<sub>50%</sub> was 84 for poor agreement, and 23 for not poor agreement. Between ULDCCT<sub>70%</sub> and LDCT<sub>50%</sub>, there were 57 features with poor agreement, and 50 with not poor agreement. Between

ULDCCT<sub>90%</sub> and LDCT<sub>50%</sub>, the number of features was 54 for not poor agreement, and 53 for poor agreement.

#### *Proportion of features with CCC >0.9 between ULDCCTs with different ASiR-V levels and LDCT*

The comparison of proportions of features with CCC >0.9 between ULDCCTs with different ASiR-V levels and LDCT is shown in *Table 2*. In SNs, there was no statistical difference for the proportion of features with CCC >0.9 between ULDCCTs with different ASiR-V levels and LDCT

**Table 3** Comparison of mean CCC values for the agreement of all features between ULDCT with different ASiR-V levels and LDCT

Variable	Group 1	Group 2	Group 3	t-value	P value
Mean CCC of SN (95% CI)	0.68 (0.64–0.73)	0.64 (0.60–0.68)	0.67 (0.62–0.72)	-5.997 <sup>a</sup> /-0.523 <sup>b</sup> /1.695 <sup>c</sup>	<0.001 <sup>a</sup> /0.602 <sup>b</sup> /0.093 <sup>c</sup>
Mean CCC of pGGN (95% CI)	0.61 (0.55–0.66)	0.76 (0.72–0.81)	0.79 (0.75–0.82)	11.489 <sup>a</sup> /10.166 <sup>b</sup> /1.992 <sup>c</sup>	<0.001 <sup>a</sup> / $<0.001^b$ /0.0489 <sup>c</sup>

ULDCT, ultralow-dose computed tomography; LDCT, low-dose computed tomography; SN, solid nodule; pGGN, pure ground-glass nodule; CCC, concordance correlation coefficient; CI, confidence interval; Group 1, agreement between ULDCT with ASiR-V 50% vs. LDCT with ASiR-V 50%; Group 2, agreement between ULDCT with ASiR-V 70% vs. LDCT with ASiR-V 50%; Group 3, agreement between ULDCT with ASiR-V 90% vs. LDCT with ASiR-V 50%. <sup>a</sup>Paired samples t-test for Group 1 and Group 2; <sup>b</sup>Paired samples t-test for Group 1 and Group 3; <sup>c</sup>Paired samples t-test for Group 2 and Group 3.

( $P=0.325$ ). In pGGNs, the proportion of features with CCC  $>0.9$  between ULDCT<sub>70%</sub> and LDCT<sub>50%</sub> was almost the same as that between ULDCT<sub>90%</sub> and LDCT<sub>50%</sub> ( $P=0.584$ ). The two proportions above were all higher than that between ULDCT<sub>50%</sub> and LDCT<sub>50%</sub> ( $P<0.001$ ).

#### Comparison of mean CCC values between ULDCTs with different ASiR-V levels and LDCT

The comparison of mean CCC values between ULDCTs with different ASiR-V levels and LDCT in both SNs and pGGNs is shown in Table 3. In SNs, the mean CCC for the agreement between ULDCT<sub>90%</sub> and LDCT<sub>50%</sub> was  $0.67\pm 0.26$ , which was not statistically different from that for ULDCT<sub>50%</sub> vs. LDCT<sub>50%</sub> ( $0.68\pm 0.24$ ) and that for ULDCT<sub>70%</sub> vs. LDCT<sub>50%</sub> ( $0.64\pm 0.21$ ) ( $P>0.05$ ). However, the mean CCC between ULDCT<sub>50%</sub> and LDCT<sub>50%</sub> was slightly higher than that between ULDCT<sub>70%</sub> and LDCT<sub>50%</sub> ( $P<0.001$ ).

In pGGNs, the mean CCC for the agreement between ULDCT<sub>90%</sub> and LDCT<sub>50%</sub> was  $0.79\pm 0.19$ , which was higher than that for ULDCT<sub>70%</sub> vs. LDCT<sub>50%</sub> ( $0.76\pm 0.24$ ) and that for ULDCT<sub>50%</sub> vs. LDCT<sub>50%</sub> ( $0.61\pm 0.28$ ) ( $P<0.05$ ). Additionally, the mean CCC between ULDCT<sub>70%</sub> and LDCT<sub>50%</sub> was also higher than that between ULDCT<sub>50%</sub> and LDCT<sub>50%</sub> ( $P<0.001$ ).

## Discussion

To our knowledge, this is the first study to show the effect of ASiR-V levels on the reproducibility of CT radiomic features between ULDCT and LDCT. In this study, we found that ASiR-V levels had a pronounced effect on the radiomic features of ULDCT (including first-order statistical, texture, and structural features), with pGGNs

being more significantly affected than SNs. Meanwhile, the increase in ASiR-V levels could enhance the reproducibility of radiomic features between ULDCT and LDCT.

Because of the differences in acquisition parameters and reconstruction techniques of CT images, there was controversial about the reproducibility of CT radiomic features. In a study on the effect of reconstruction algorithms on CT radiomic features of pulmonary tumors, Kim *et al.* (32) found that 66.7 (4/6) first-order tumor intensity features and 75% (3/4) GLCM features were significantly influenced by the noise reduction strength of Sinogram Affirmed Iterative Reconstruction (SAFIRE) from level 3 to level 5. In the meantime, Prezzi *et al.* (21) investigated whether ASiR affected CT radiomic quantification in primary colorectal cancer and found that incremental ASiR levels determined a significant change in most statistical radiomic features. Our results also indicated that the ULDCT radiomic features would be strongly influenced by the change in ASiR-V levels in both SN and pGGN. There were at most 86 features with CCC $<0.9$  in SN, and the number in pGGN reached at most 79, which was more than 73% of the total features. These studies indicated that CT radiomic quantification would be markedly influenced by the change in ASiR levels, similar to other IR algorithms such as SAFIRE and ASiR.

Except for reconstruction algorithms, the reproducibility of CT radiomic features will also be influenced by the radiation dose of CT scan (33–35). In a study on the influence of radiation dose and CT reconstruction setting on the reproducibility of CT radiomic features within the same patient, Meyer *et al.* (33) found that radiation dose had an obvious effect on the reproducibility of radiomic features, and the percentage of radiomic features deemed reproducible was reduced to 18% (19/106) from the dose level 100% to dose level 25%. Another study also found that

the reduction of radiation dose from 120mAs to 30mAs led to significant changes in 90% (18/20) radiomic features (34). In our study, the reproducibility of radiomic features between ULDCT<sub>50%</sub> and LDCT<sub>50%</sub> markedly decreased when the ED of ULDCT was reduced to approximately 20% of LDCT. The mean CCC value for the agreement of all features between ULDCT<sub>50%</sub> and LDCT<sub>50%</sub> was approximately 0.68 in SN and 0.61 in pGGN. In addition, the proportion of features with CCC <0.9 was as high as 78.5% to 81.3%, which aligned with the results of the two studies above. All these results suggest that the reproducibility of radiomic features between ULDCT and LDCT will significantly decrease with a reduction in radiation dose.

It is well known that the noise of an image will increase with the reduction of radiation dose. In our study, the reduction of radiation dose also led to significant changes in the reproducibility of radiomic features between ULDCT and LDCT. However, some studies have indicated that increasing ASiR-V levels can lead to the reduction of image noise and improve the contrast-to-noise ratio (36). In view of this fact, we hypothesized that incremental ASiR-V levels may increase the reproducibility of radiomic features between ULDCT and LDCT.

In our study, we extensively assessed the agreement of radiomic features between ULDCT with different ASiR-V levels and LDCT in both SN and pGGN. In SN, the agreement of radiomic features between ULDCT and LDCT underwent a slight change when ASiR-V levels of ULDCT changed and the radiation dose of the two CT scans remained steady. Despite the ASiR-V level up to 90% from 50%, the magnitude of variation in the mean CCC value for the agreement of all features between ULDCT and LDCT was less than 0.04. In addition, the proportion of features with CCC >0.9 between ULDCT with different ASiR-V levels and LDCT did not strongly increase.

However, the agreement of radiomic features between ULDCT and LDCT increased greatly with increasing ASiR-V levels for ULDCT in pGGN. The mean CCC value for the agreement of all features between ULDCT<sub>90%</sub> and LDCT<sub>50%</sub> increased by 0.18 compared with that between ULDCT<sub>50%</sub> and LDCT<sub>50%</sub>, with a 30% increase. Although the ED of ULDCT was only 21.4% that of LDCT, the mean CCC value for the agreement of all features between ULDCT<sub>90%</sub> and LDCT<sub>50%</sub> was as high as 0.79. In the meantime, the proportion of features with CCC >0.9 between ULDCT<sub>90%</sub> and LDCT<sub>50%</sub> was up to 50.5% compared with that between ULDCT<sub>50%</sub> and LDCT<sub>50%</sub>.

For the obviously different effect between SN and pGGN, it may be explained that the lower intensity of pGGN was more sensitive to changes in image noise. In conclusion, the results of our study indicate that incremental ASiR-V levels, to some degree, can reduce the negative effect of dose reduction on the reproducibility of LDCT radiomic features and enhance the reproducibility of radiomic features between ULDCT and LDCT. Meanwhile, it has been recently shown that CT image reconstruction algorithms not only affect the reproducibility of radiomic features, but also affect the diagnostic performance of radiomics models (37). Thus, the difference in diagnostic performance of the radiomics models between LDCT and ULDCT may be narrowed to some extent by increasing ASiR-V levels to enhance the reproducibility of radiomic features.

This study had some limitations. First, levels of ASiR-V for ULDCT in our study only included 50%, 70%, and 90%, which did not cover the range from 0% to 100%. Afadzi *et al.* (16) recommended that ASiR-V levels below 70% may be appropriate for LDCT and ULDCT. Besides, levels of ASiR-V from 40% to 60% were recommended as the reconstruction levels for chest CT in another study (36). Thus, we chose the most likely levels of ASiR-V (including 50%, 70%, and 90%), which may be used for LDCT and ULDCT in practical applications. Second, our study only focused on the comparison of reproducibility of radiomic features between ULDCT and LDCT in both SNs and pGGNs, not covering PSNs. Third, whether the difference in reproducibility of radiomic features between ULDCT and LDCT can affect the diagnostic performance of radiomics models based on images of two scans needs to be explored. Therefore, more types of pulmonary nodules need to be included and the effect of ASiR-V levels on the diagnostic performance of radiomics models based on images of ULDCT and LDCT should be investigated in the future.

## Conclusions

In conclusion, we have confirmed that ASiR-V levels can also significantly affect the quantification of radiomics features computed at ULDCT in pulmonary nodules, similar to the radiation dose, and that pGGN was more sensitive than SN. The increase in ASiR-V levels could enhance the reproducibility of radiomic features between ULDCT and LDCT to some degree. In the future, higher ASiR-V levels may be taken when radiomics models

based on the ULDCT images are used in the diagnosis of pulmonary nodules.

## Acknowledgments

We would like to thank Editage ([www.editage.cn](http://www.editage.cn)) for English language editing.

*Funding:* None.

## Footnote

*Conflicts of Interest:* All authors have completed the ICMJE uniform disclosure form (available at <http://dx.doi.org/10.21037/qims-20-932>). The authors have no conflicts of interest to declare

*Ethical Statement:* This study was approved by the institutional review board of our department (NO. M2019296), and informed consent was obtained from the participants.

*Open Access Statement:* This is an Open Access article distributed in accordance with the Creative Commons Attribution-NonCommercial-NoDerivs 4.0 International License (CC BY-NC-ND 4.0), which permits the non-commercial replication and distribution of the article with the strict proviso that no changes or edits are made and the original work is properly cited (including links to both the formal publication through the relevant DOI and the license). See: <https://creativecommons.org/licenses/by-nc-nd/4.0/>.

## References

- Gillies RJ, Kinahan PE, Hricak H. Radiomics: Images Are More than Pictures, They Are Data. *Radiology* 2016;278:563-77.
- Kim H, Park CM, Goo JM, Wildberger JE, Kauczor HU. Quantitative Computed Tomography Imaging Biomarkers in the Diagnosis and Management of Lung Cancer. *Invest Radiol* 2015;50:571-83.
- Fan L, Fang M, Li Z, Tu W, Wang S, Chen W, Tian J, Dong D, Liu S. Radiomics signature: a biomarker for the preoperative discrimination of lung invasive adenocarcinoma manifesting as a ground-glass nodule. *Eur Radiol* 2019;29:889-97.
- Koyasu S, Nishio M, Isoda H, Nakamoto Y, Togashi K. Usefulness of gradient tree boosting for predicting histological subtype and EGFR mutation status of non-small cell lung cancer on 18F FDG-PET/CT. *Ann Nucl Med* 2020;34:49-57.
- Beig N, Khorrani M, Alilou M, Prasanna P, Braman N, Orooji M, Rakshit S, Bera K, Rajiah P, Ginsberg J, Donatelli C, Thawani R, Yang M, Jacono F, Tiwari P, Velcheti V, Gilkeson R, Linden P, Madabhushi A. Perinodular and Intranodular Radiomic Features on Lung CT Images Distinguish Adenocarcinomas from Granulomas. *Radiology* 2019;290:783-92.
- Wilson R, Devaraj A. Radiomics of pulmonary nodules and lung cancer. *Transl Lung Cancer Res* 2017;6:86-91.
- Thawani R, McLane M, Beig N, Ghose S, Prasanna P, Velcheti V, Madabhushi A. Radiomics and radiogenomics in lung cancer: A review for the clinician. *Lung Cancer* 2018;115:34-41.
- Aberle DR, Adams AM, Berg CD, Black WC, Clapp JD, Fagerstrom RM, Gareen IF, Gatsonis C, Marcus PM, Sicks JD. Reduced lung-cancer mortality with low-dose computed tomographic screening. *N Engl J Med* 2011;365:395-409.
- Delzell DA, Magnuson S, Peter T, Smith M, Smith BJ. Machine Learning and Feature Selection Methods for Disease Classification With Application to Lung Cancer Screening Image Data. *Front Oncol* 2019;9:1393.
- Mao L, Chen H, Liang M, Li K, Gao J, Qin P, Ding X, Li X, Liu X. Quantitative radiomic model for predicting malignancy of small solid pulmonary nodules detected by low-dose CT screening. *Quant Imaging Med Surg* 2019;9:263-72.
- Hawkins S, Wang H, Liu Y, Garcia A, Stringfield O, Krewer H, Li Q, Cherezov D, Gatenby RA, Balagurunathan Y, Goldgof D, Schabath MB, Hall L, Gillies RJ. Predicting Malignant Nodules from Screening CT Scans. *J Thorac Oncol* 2016;11:2120-8.
- Ohno Y, Koyama H, Seki S, Kishida Y, Yoshikawa T. Radiation dose reduction techniques for chest CT: Principles and clinical results. *Eur J Radiol* 2019;111:93-103.
- Lell MM, Kachelrieß M. Recent and Upcoming Technological Developments in Computed Tomography: High Speed, Low Dose, Deep Learning, Multienergy. *Invest Radiol* 2020;55:8-19.
- Nishio M, Koyama H, Ohno Y, Negi N, Seki S, Yoshikawa T, Sugimura K. Emphysema Quantification Using Ultralow-Dose CT With Iterative Reconstruction and Filtered Back Projection. *AJR Am J Roentgenol* 2016;206:1184-92.
- Euler A, Solomon J, Marin D, Nelson RC, Samei E. A Third-Generation Adaptive Statistical Iterative

- Reconstruction Technique: Phantom Study of Image Noise, Spatial Resolution, Lesion Detectability, and Dose Reduction Potential. *AJR Am J Roentgenol* 2018;210:1301-8.
16. Afadzi M, Lysvik EK, Andersen HK, ACT M. Ultra-low dose chest computed tomography: Effect of iterative reconstruction levels on image quality. *Eur J Radiol* 2019;114:62-8.
  17. Messerli M, Kluckert T, Knitel M, Wälti S, Desbiolles L, Rengier F, Warschkow R, Bauer RW, Alkadhi H, Leschka S, Wildermuth S. Ultralow dose CT for pulmonary nodule detection with chest x-ray equivalent dose - a prospective intra-individual comparative study. *Eur Radiol* 2017;27:3290-9.
  18. Jin S, Zhang B, Zhang L, Li S, Li S, Li P. Lung nodules assessment in ultra-low-dose CT with iterative reconstruction compared to conventional dose CT. *Quant Imaging Med Surg* 2018;8:480-90.
  19. Ye K, Zhu Q, Li M, Lu Y, Yuan H. A feasibility study of pulmonary nodule detection by ultralow-dose CT with adaptive statistical iterative reconstruction-V technique. *Eur J Radiol* 2019;119:108652.
  20. Miller AR, Jackson D, Hui C, Deshpande S, Kuo E, Hamilton GS, Lau KK. Lung nodules are reliably detectable on ultra-low-dose CT utilising model-based iterative reconstruction with radiation equivalent to plain radiography. *Clin Radiol* 2019;74:409.e17-409.e22.
  21. Prezzi D, Owczarczyk K, Bassett P, Siddique M, Breen DJ, Cook GJR, Goh V. Adaptive statistical iterative reconstruction (ASiR) affects CT radiomics quantification in primary colorectal cancer. *Eur Radiol* 2019;29:5227-35.
  22. Kim H, Goo JM, Ohno Y, Kauczor HU, Hoffman EA, Gee JC, Beek EJRV. Effect of Reconstruction Parameters on the Quantitative Analysis of Chest Computed Tomography. *J Thorac Imaging* 2019;34:92-102.
  23. Zhao W, Zhang W, Sun Y, Ye Y, Yang J, Chen W, Gao P, Li J, Li C, Jin L, Wang P, Hua Y, Li M. Convolution kernel and iterative reconstruction affect the diagnostic performance of radiomics and deep learning in lung adenocarcinoma pathological subtypes. *Thorac Cancer* 2019;10:1893-903.
  24. Solomon J, Mileto A, Nelson RC, Roy CK, Samei E. Quantitative Features of Liver Lesions, Lung Nodules, and Renal Stones at Multi-Detector Row CT Examinations: Dependency on Radiation Dose and Reconstruction Algorithm. *Radiology* 2016;279:185-94.
  25. Midya A, Chakraborty J, Gönen M, RKG D, Simpson AL. Influence of CT acquisition and reconstruction parameters on radiomic feature reproducibility. *J Med Imaging (Bellingham)* 2018;5:011020.
  26. Mileto A, Guimaraes LS, McCollough CH, Fletcher JG, Yu L. State of the Art in Abdominal CT: The Limits of Iterative Reconstruction Algorithms. *Radiology* 2019;293:491-503.
  27. MacMahon H, Naidich DP, Goo JM, Lee KS, Leung ANC, Mayo JR, Mehta AC, Ohno Y, Powell CA, Prokop M, Rubin GD, Schaefer-Prokop CM, Travis WD, Schil PEV, Bankier AA. Guidelines for Management of Incidental Pulmonary Nodules Detected on CT Images: From the Fleischner Society 2017. *Radiology* 2017;284:228-43.
  28. Deak PD, Smal Y, Kalender WA. Multisection CT protocols: sex- and age-specific conversion factors used to determine effective dose from dose-length product. *Radiology* 2010;257:158-66.
  29. Lambin P, Rios-Velazquez E, Leijenaar R, Carvalho S, Stiphout RGPMV, Granton P, Zegers CML, Gillies R, Boellard R, Dekker A, Aerts HJWL. Radiomics: extracting more information from medical images using advanced feature analysis. *Eur J Cancer* 2012;48:441-6.
  30. Liu J, Tang W, Chen G, Lu Y, Feng C, Tu XM. Correlation and agreement: overview and clarification of competing concepts and measures. *Shanghai Arch Psychiatry* 2016;28:115-20.
  31. McBride GB (2005). A proposal for strength-of-agreement criteria for Lin's concordance correlation coefficient. NIWA Client Report: HAM2005-062. Available online: <http://www.medcalc.org/download/pdf/McBride2005.pdf>. Accessed 18 Dec 2020.
  32. Kim H, Park CM, Lee M, Park SJ, Song YS, Lee JH, Hwang EJ, Goo JM. Impact of Reconstruction Algorithms on CT Radiomic Features of Pulmonary Tumors: Analysis of Intra- and Inter-Reader Variability and Inter-Reconstruction Algorithm Variability. *PLoS One* 2016;11:e0164924.
  33. Meyer M, Ronald J, Vernuccio F, Nelson RC, Ramirez-Giraldo JC, Solomon J, Patel BN, Samei E, Marin D. Reproducibility of CT Radiomic Features within the Same Patient: Influence of Radiation Dose and CT Reconstruction Settings. *Radiology* 2019;293:583-91.
  34. Kim YJ, Lee HJ, Kim KG, Lee SH. The Effect of CT Scan Parameters on the Measurement of CT Radiomic Features: A Lung Nodule Phantom Study. *Comput Math Methods Med* 2019;2019:8790694.
  35. Buch K, Li B, Qureshi MM, Kuno H, Anderson SW, Sakai O. Quantitative Assessment of Variation in CT Parameters

- on Texture Features: Pilot Study Using a Nonanatomic Phantom. *AJNR Am J Neuroradiol* 2017;38:981-5.
36. Tang H, Yu N, Jia Y, Yu Y, Duan H, Han D, Ma G, Ren C, He T. Assessment of noise reduction potential and image quality improvement of a new generation adaptive statistical iterative reconstruction (ASIR-V) in chest CT. *Br J Radiol* 2018;91:20170521.
37. Kim H, Park CM, Gwak J, Hwang EJ, Lee SY, Jung J, Hong H, Goo JM. Effect of CT Reconstruction Algorithm on the Diagnostic Performance of Radiomics Models: A Task-Based Approach for Pulmonary Subsolid Nodules. *AJR Am J Roentgenol* 2019;212:505-12.

**Cite this article as:** Ye K, Chen M, Zhu Q, Lu Y, Yuan H. Effect of adaptive statistical iterative reconstruction-V (ASiR-V) levels on ultra-low-dose CT radiomics quantification in pulmonary nodules. *Quant Imaging Med Surg* 2021;11(6):2344-2353. doi: 10.21037/qims-20-932

**Table S1** Summary and brief description of all the 107 CT radiomic features extracted

Feature type	Method	Parameters
First order feature	Describe the distribution of voxel intensities within the image region defined by the mask through commonly used and basic metrics	Interquartile Range, Skewness, Uniformity, Median, Energy, Mean Absolute Deviation, Entropy, Range, Root Mean Squared, Robust Mean Absolute Deviation, Minimum, Total Energy, Variance, Kurtosis, 10Percentile, Mean, Maximum, 90Percentile
Shape feature(3D)	Describe the three-dimensional size and shape of the region of interest only on the non-derived image and mask	Voxel Volume, Flatness, Major Axis Length, Mesh Volume, Maximum 2D Diameter Slice, Sphericity, Surface Volume Ratio, Elongation, Minor Axis Length, Maximum 2D Diameter Row, Maximum 3D Diameter, Least Axis Length, Surface Area, Maximum2D Diameter Column
GLCM	Describe the second-order joint probability function of an image region constrained by the mask	Joint Average, Sum Average, Joint Entropy, Cluster Shade, Maximum Probability, Idmn, Joint Energy, Contrast, Difference Entropy, Inverse Variance, Idn, Difference Variance, Cluster Prominence, Idm, Correlation, Auto correlation, Sum Entropy, MCC, Sum Squares, Imc2, Imc1, Difference Average, Id, Cluster Tendency
GLDM	Quantify gray level dependencies, which are defined as the number of connected voxels within distance $\delta$ that are dependent on the center voxel	Gray Level Variance, High Gray Level Emphasis, Dependence Entropy, Dependence Non Uniformity, Gray Level Non Uniformity, Small Dependence Emphasis, Small Dependence High Gray Level Emphasis, Dependence Non Uniformity Normalized, Large Dependence Emphasis, Large Dependence Low Gray Level Emphasis, Dependence Variance, Large Dependence High Gray Level Emphasis, Small Dependence Low Gray Level Emphasis, Low Gray Level Emphasis
GLRLM	Quantify gray level runs, which are defined as the length in number of pixels, of consecutive pixels that have the same gray level value	Short Run Low Gray Level Emphasis, Gray Level Variance, Low Gray Level Run Emphasis, Gray Level Non Uniformity Normalized, Run Variance, Gray Level Non Uniformity, Long Run Emphasis, Short Run High Gray Level Emphasis, Run Length Non Uniformity, Short Run Emphasis, Long Run High Gray Level Emphasis, Run Percentage, Long Run Low Gray Level Emphasis, Run Entropy, High Gray Level Run Emphasis, Run Length Non Uniformity Normalized
GLSZM	Quantify gray level zones which were defined as the number of connected voxels that share the same gray level intensity	Gray Level Variance, Zone Variance, Gray Level Non Uniformity Normalized, Size Zone Non Uniformity Normalized, Size Zone Non Uniformity, Gray Level Non Uniformity, Large Area Emphasis, Small Area High Gray Level Emphasis, Zone Percentage, Large Area Low Gray Level Emphasis, Large Area High Gray Level Emphasis, High Gray Level Zone Emphasis, Small Area Emphasis, Low Gray Level Zone Emphasis, Zone Entropy, Small Area Low Gray Level Emphasis
NGTDM	Quantify the difference between a gray value and the average gray value of its neighbours within distance $\delta$	Coarseness, Complexity, Strength, Contrast, Busyness

GLCM, gray level co-occurrence matrix; GLDM, gray level dependence matrix; GLRLM, gray level run length matrix; GLSZM, gray level size zone matrix; NGTDM, neighbouring gray tone difference matrix.